Robust Surface Light Scattering Spectroscopy for Fluid Interfaces

Angelo S Visco[1], Alan R Baldwin[1], Alexander I Belgovskiy[2], J Adin Mann[3], William V Meyer[4], Anthony E Smart[4], Nabin K Thapa[1], Elizabeth K Mann[1]

[1] Department of Physics, Kent State University, USA
[2] Analiza, Inc., USA
[3] Department of Chemical and Biomolecular Engineering, Case Western Reserve University, USA
[4] Scattering Solutions Inc., USA

E-mail: emann@kent.edu

Received xxxxxx
Accepted for publication xxxxxx
Published xxxxxx

Abstract

Surface Light Scattering Spectroscopy (SLSS) can characterize the dynamics of an interface between two immiscible fluids by measuring the frequency spectrum of coherent light scattered from thermophysical fluctuations – 'ripplons'. In principle, and for many interfaces, SLSS can simultaneously measure surface tension and viscosity, with the potential for higher-order properties, such as surface elasticity and bending moments. Previously, this has been challenging. We describe and present some measurements from an instrument with improvements in optical design, specimen access, vibrational stability, signal-to-noise ratio, electronics, and data processing. Quantitative improvements include total internal reflection at the interface to enhance the typically available signal by a factor of order 40 and optical improvements that minimize adverse effects of sloshing induced by external vibrations. Information retrieval is based on a comprehensive surface response function, an instrument function, which compensates for real geometrical and optical limitations, and processing of almost real-time data to report results and their likely accuracy. Detailed models may be fit to the power spectrum in real-time. The raw one-dimensional digitized data stream is archived to allow post-experiment processing. This paper reports a system design and implementation that offers substantial improvements in accuracy, simplicity, ease of use, and cost. The presented data are for systems in regions of low viscosity where the ripplons are underdamped, but the hardware described is more widely applicable.

Keywords: Instrumentation, Surface Light Scattering, SLS, Fluid Interfaces, Capillary Waves, Ripplons, Surface Tension, Viscosity

1. Introduction

This paper together with its supplementary materials serves two purposes: 1) to present a new design of surface light scattering spectrometer that is robust, accurate, and easy to use and 2) to describe how to implement this design.

Surface Light Scattering Spectroscopy (SLSS) can characterize non-invasively properties of an interface between two fluids of different refractive index. Since its introduction 60 years ago, several groups [1–12] have evolved and exploited the technique with increasing accuracy and precision. However, the technique remains under-used because it is "delicate and not simple to operate" [1]. Sloshing due to mechanical vibrations causes the beam to drift over or beyond the detector even with good antivibration tables. Through systematic analysis, technical improvement, and innovation, we have extended the usefulness of this technique by increasing the available signal, improving resistance to external perturbations, and applying surface response and instrument functions to reduce systematic errors.

Our significant novelty is the combination of (1) an improved configuration using Total Internal Reflection (TIR), to enhance the signal by a factor of ~40 (see Supplementary Materials, eq. S5), (2) a diffraction-limited optical system optimized to reduce the effect of inevitable 'sloshing' caused by vibration under typical laboratory conditions, (3) the ability to analyse the signal and present data in real-time to build confidence in experimental operation, and (4) the ability to record the complete real-time signal, with its necessary provenance, for further analysis of the entire data stream or of selected segments, especially useful for evolving systems. This combination allows us to present results enhanced over published literature that we have found [1,13–38]. The resulting innovative instrument is both more precise and more accurate, with resistance to sloshing, and relative ease of use. The significance is that this technique is now practical without requiring extraordinarily quiet environments and good vibration-control tables. The results presented in this paper were taken in a third-floor lab next to an active construction site, a capability unheard of before the improvements detailed in this paper.

Fluid interfaces are everywhere. SLSS is typically used to measure surface tension, or energy per unit area, of a surface, which is basically flat to within fractions of a nanometre; it can also yield bulk viscosity and surface viscoelastic coefficients. Knowledge of such interfacial properties is important in biology and in industry, characterizing the stability of emulsions and foams, dynamics within cell membranes, the consequences of Marangoni forces, the control of reflow and wave soldering, etc.

Surface tension can be measured by several classical methods, including capillary rise, the Wilhelmy plate, the du Noüy ring, and drop-shape techniques [2–4]. However, all these involve contact of the fluids with a solid, and most depend on controlling or measuring the contact angle. With contact methods, the surrounding environment and the possibility of contamination can make measurements difficult and sometimes unreliable.

Being non-contact, SLSS avoids these difficulties and accurately measures a wide range of surface tensions, even down to low values close to a critical point [5].

2. Basic Principles of SLSS

2.1. Capillary Waves

SLSS collects fluctuating light scattered by ripplons, thermophysically generated capillary waves present at any interface between two fluids, and generates a temporal power spectrum whose characteristics depend upon interfacial and volume properties via the Surface Response Function (SRF) [6,7]. A fluid interface has both an intrinsic roughness caused by the thermally excited ripplons, and an intrinsic thickness caused by a density gradient close to the surface. For molecularly thin interfaces, convention replaces the interfacial region with a mathematically discontinuous Gibbs surface [8–10]. Analysis of scattered light considers the interface as this mathematical surface of zero thickness, while, even far from a critical point, the true interfacial behaviour extends over a finite region on a molecular scale. Indeed, considerable effort

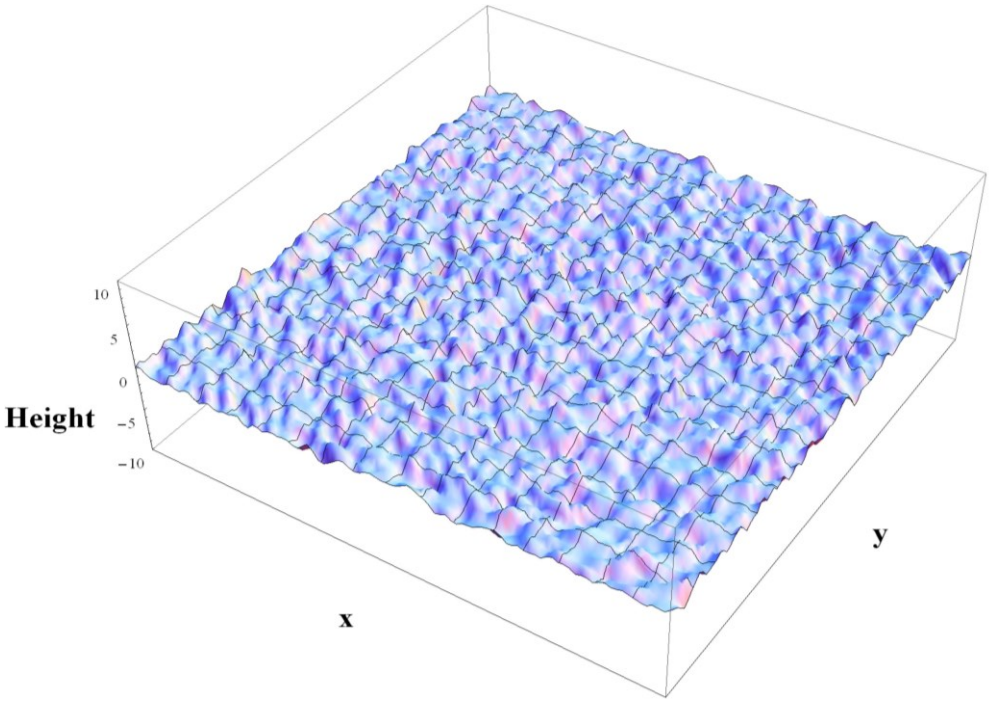

Figure 1. Artist's impression of a thermally perturbed surface – vertical dimension highly magnified.

has been spent in separating consequences of intrinsic thickness and thermodynamically excited roughness of an interface [11].

Attempts have been made to observe ripplons directly [12]. **Figure 1** is an artist's impression of how a ripplon covered surface might differ from a flat reference surface. The vertical height, z(x,y,t), typically only fractions of a nanometre, satisfies stochastic partial differential equations that involve the differential geometry of mass, momentum, and energy conservation at the interface. The instrument yields a power spectrum that is well described by models based upon Fourier and Laplace transforms of stochastic functions discussed by J. Mann, et al. [39].

The surface disturbance has a distribution of spatial wavelengths, amplitudes, and phases described by a set of wave vectors $\vec{q}$ in the mean plane of the interface, traditionally the Gibbs surface. The vertical average displacement, $\sqrt{\langle z_q^2 \rangle}$, of the ripplons with wavenumber q, is typically orders of magnitude less than the wavelength, $2\pi/q$, and can be estimated from the excess surface area and gravitational energy by the equipartition theorem [39,40] resulting in the formula

$$\langle z_q^2 \rangle = \frac{k_B T}{(\gamma\, q^2 + \Delta\rho\, g) A_0} \qquad (1)$$

where γ is the surface tension, $\Delta\rho$ is the density difference between the two bulk fluids, g is the gravitational acceleration, T is the absolute temperature, k_B is Boltzmann's constant, and A_0 is the projected area of the measured surface onto the horizontal plane, expressed in self consistent units. This equation assumes that the different values of $\vec{q}$ correspond to independent normal modes.

The mean squared displacement from a plane is found by integrating equation (1) over all physical values of the wave vector, which for a simple low-viscosity liquid such as acetone in equilibrium with its vapor is ~0.7 nm [11]. To measure the temporal properties of $\vec{q}$ with this instrument, we now introduce a vector $\vec{k}$ to represent a parallel grid projected onto the surface. Such a grating pattern diffracts light into several orders, one of which is typically selected to amplify the natural $\vec{q}$ scattering in only that chosen direction. Measurement of the temporal variation of this single order indicates the properties of surface scattering in a mean specific direction where $\vec{k}$ may be viewed as a selective filter on $\vec{q}$. Coherent optical amplification over a narrow range of values near $\vec{k}$ makes possible the measurement of scattering at high angles, whose already low intensity reduces as $\sim 1/q^4$.

Because the grating image selects only a narrow range of $\vec{q}$, the relevant resolved surface displacement height away from the critical point is even smaller – closer to picometers, less than the size of a molecule. Substantial literature [7,40] shows that classical continuum theory still describes experimental findings, even in quantum fluids such as liquid helium [41].

2.2. Extracting Interface Properties with the Surface Response Function

Surface disturbances seek to return to an energetically minimal flat surface, but are prevented from doing so by continuous excitation by temperature-driven entropy fluctuations leading to local density variations, giving a time dependence to the surface contour. The temporal frequency, typically varying with spatial frequency as $q^{3/2}$, observable at any scattering angle for which there is sufficient light, depends dominantly on both surface tension and density.

The surface tension and other surface and bulk properties can be extracted from the power spectrum (**Figure 2**) using some simplifying assumptions. First, the wavelength in the surface greatly exceeds the wave height, so the slopes of surface ripplons are exceedingly small. Second, gravitational effects in equation (1) are not significant and may be disregarded. Finally, the fluid dynamics is modelled as a continuous velocity field, which can be divided into two components: the gradient of a scalar potential and the curl of a vector stream function, in analogy with electromagnetic and other fields. Our analysis uses a full and rigorous treatment [39], whereas historically the stream function component has been neglected giving only qualitatively reasonable results, and then only for sufficiently low viscosities, as shown in Section 6.1.

The SRF also includes higher-order visco-elastic and bending effects, which are not available through the historical approach. Even without including these higher-order effects, the SRF provides excellent fits, with low and random residuals, for fluids of sufficiently low viscosity discussed here, as shown in **Figure 2** and **Figure 6** through **Figure 8**. The low residuals imply that there is little information about higher order effects, which is expected to be negligible for such simple fluids. Where residuals are larger, for example

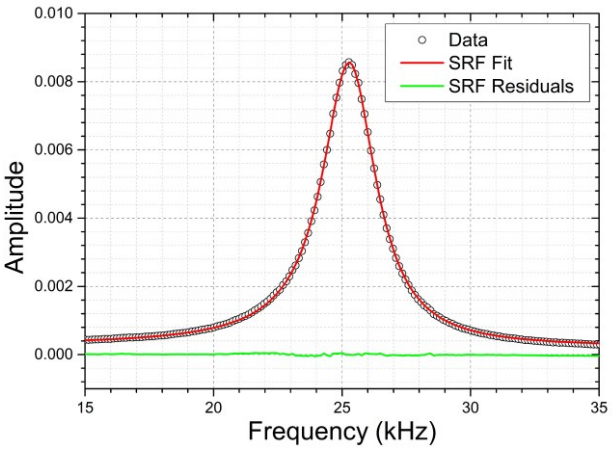

Figure 2. Power spectrum of pentane at 19.95°C with a 1000/cm grating, 1 µs sampling time, and 10-minute experiment duration. Surface Response Function (SRF) fit with an applied instrument function.

with a thin film at the interface, they may allow the inference higher order effects.

Further improvements to these measurements are available with an 'instrument function' that addresses and partially compensates for optical properties of the system implementation as described in Sections 4 and 6.2, respectively, and in the Supplementary Materials Section S4.

2.3. Dimensionless Parameters and Approximations

Dimensionless parameters and simple functions derived without the contribution from the stream function can usefully describe different power spectral regimes and develop an intuitive understanding of the behaviour of the experimental spectra. When the viscosity is sufficiently high the separation of values for surface tension and viscosity becomes difficult or impractical. Further extension of the Instrument Function presented here offers the promise of yet additional improvement, but is beyond the scope of this paper. Currently the onset of the regime where surface tension and viscosity may be simultaneously measured to reasonable accuracy can be usefully predicted by a dimensionless parameter y^*, which depends on the spatial frequency q. This dimensionless parameter characterizing ripplon damping is

$$y^* = \frac{\gamma\,\rho}{q\,\eta^2} \qquad (2)$$

where ρ is the liquid density, η is the viscosity of the liquid, with both the viscosity and density of the vapor assumed negligible [40]. The system is close to critically damped when $y^* \cong 0.58$. As y^* decreases the waves become progressively more heavily damped and as y^* increases far beyond 0.58, the underdamped waves become more oscillatory. For low viscosity, where y^* greatly exceeds 0.58, the power spectral peak narrows and moves away from zero, improving accuracy of fitting the model and hence the reported measurements.

The historical approximation assumes irrotational flow, so that the stream function may be ignored [39,40]; this gives a valuable first approximation to the power spectrum when $y^* \gg 0.58$, which is the focus of this paper. This approximation simplifies the dispersion relationship to

$$\omega_q^2 = \frac{\gamma\,|q^3|}{\rho}\,, \qquad (3)$$

where ω_q is the frequency associated with the wave number q, and gives a time constant

$$\tau = \frac{\rho}{2\,\eta\,q^2}\,. \qquad (4)$$

Note that within the approximations leading to equations (3) and (4), the power spectrum would be a Lorentzian, with a central frequency given by equation (3) and a width given by $1/\tau$. As liquid viscosity increases, the spectrum deviates progressively more from this ideal. A dimensionless parameter,

$$Y_1 = \frac{\rho\,\omega_c^2}{\gamma\,|q^3|}, \qquad (5)$$

where ω_c is the frequency of the power spectral peak, determines how badly the system fails the Lorentzian approximation. When $Y_1 \approx 1$, surface tension and viscosity can be determined nearly independently: the peak position is determined mostly by the surface tension, while the width of the distribution is determined mostly by the viscosity. As Y_1 decreases, however, surface tension and viscosity are increasingly entangled in both the peak position and width, and determining either unambiguously may require knowledge of the other (see **Figure 5** and **Table 1** in the Results Section 6.2). Using the comprehensive SRF rather than the conventional Lorentzian yields more accurate results.

2.4. Light Scattering

As discussed in Section 2.1, in SLSS the plane wave from a laser is scattered by capillary waves. To obtain the power spectrum of the capillary waves, we condition (see Supplementary Materials Section S3 and S5), digitize the data stream, and correlate the scattered light detected over the small range of wavenumbers amplified by the first-order beam diffracted by the grating from the same coherent source. Capillary waves act like a thin phase screen, so our phase grating selects a plane wave vector $\vec{k}$ from all possible radial wave vectors $\vec{q}$ [42,43]. For underdamped ripplons, this not only amplifies the signal, but shifts the spectral peak away from zero, allowing determination of the thermophysical properties by fitting an appropriate model.

Further details, essential for properly implementing the instrument and analysing the data obtained from it, may be found in Section S2 of the Supplementary Materials.

3. SLSS Instrument

A photograph of the experimental setup, **Figure 3**, shows the cage system used for alignment and relative positioning of the optical elements. For clarity, the thermal shroud used for temperature control and insulation is omitted. This figure may be compared to the physical layout in **Figure 4**, where another mirror is placed before the detector to align the first-order diffraction spot with the centre of the detector. The functional properties of the components are summarized below with details and specifications in Section S3 of the Supplementary Materials.

Figure 4 (top), sketches the light beam paths, as an optical tunnel diagram [44] showing the important components and the near paraxial optics with distinct beam paths for illumination (red) and signal (purple). Still symbolic, but more closely physical, the bottom layout indicates sample access from beneath for TIR.

The laser output beam was well collimated to produce a spatially and temporally coherent near-circular Gaussian field

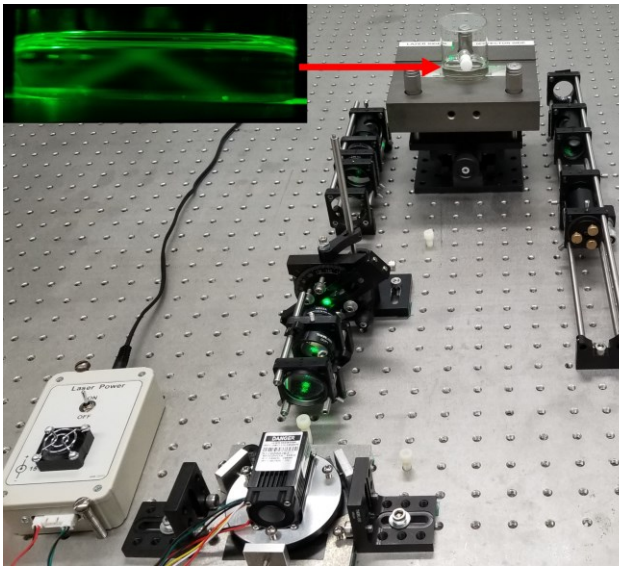

Figure 3. Experimental layout with inset showing TIR.

distribution. A phase grating is imaged onto the fluid-fluid interface. A single diffraction order is imaged onto the detector, where it coherently amplifies the light scattered from the surface at the angle selected by the chosen diffraction order.

We used either of two available blazed phase gratings with wave numbers of 500/cm and 1000/cm, chosen to make accessible a wide range of surface tension and viscosity regimes, with a tuneable power ratio of zeroth-order to first-order optimally about 75. At lower temporal frequencies, it is progressively more difficult to separate the measurements of surface tension and viscosity. At higher frequencies, with signal strength diminishing as $\sim q^{-4}$, both signal and signal-to-noise ratio are reduced. Access to higher values of $\vec{q}$ may be available by moving the detector to intercept a higher scattering order as the amplifying beam. Although the signal is much reduced, the ratio of amplifying to scattered light may be kept acceptable by translating the blazed grating. However, when using orders higher than the first, there may be additional effects from the lower, typically brighter, orders, which can merit changes to the fitting model. An alternative way to access higher $\vec{q}$ is to demagnify the grating image, preserving the power ratio but decreasing the beam size, with the possible reduction of statistical stationarity, because the higher ripplon wavelengths are de-weighted.

The diffraction-limited achromatic lens pair, individually optimized for infinite conjugates, images the grating with magnification determined by the ratio of the lens focal lengths. The disk of least confusion, which is the 'best image' focal plane, must coincide with the mean interface. However, the relative inclination, necessary for TIR, of the surface to the normal image of the grating introduces both defocusing and a scaling distortion that are accounted for by the Instrument Function. The measurement is thus sensitive to a small error in the surface placement. Alignment of the system is best performed by starting with the laser and confirming the beam properties at each successive plane of interest (see **Figure 4**).

First-surface mirrors direct the illuminating beam into the specimen cell and subsequently on to the centre of the detector. The sample is sealed in a cylindrical glass cell with an optically flat bottom, temperature controlled by shrouding all but the lower optical entrance face with a constant temperature enclosure. The cell base is optically connected to a Dove prism with a thin layer of index-matching fluid that allows for total internal reflection at the fluid surface while the entry and exit beams approach the assembly at near normal incidence without introducing further astigmatism.

Having access from beneath without significant aberrations allows TIR to increase signal strength by up to ~40 times for an acetone-air interface (Supplementary Materials eq. S5), allowing measurement of liquid/vapor for a single material, dissimilar immiscible bulk liquids, and a variety of thin layers separating different materials or phases. Access to a wide range of complex interface properties is readily available, not only where a thin layer may have interesting properties, but also where those properties may change with time as they evolve towards equilibrium. This technique has been extended to include multiple layers as thin as one or a few molecules [6,40].

The receiving lens train forms a near-diffraction-limited image of the laser source in the plane of the detector (red path on **Figure 4**), maximizing the separation between the diffraction orders compared with the radius of the image of each order, and reducing Seidel aberrations of the zero-order beam from spilling light into the higher orders. Optimizing aberrations is also a trade-off between the ideal performance of the receiving lens group in terms of the Strehl ratio of the source image (sloshing sensitivity), and the accuracy of the Fourier transform between the inclined surface and the detector plane (Section 6.3). The laser power is adjusted with neutral density filters to illuminate the PIN diode detector with 8-12 μW, below the damage or aging threshold and where the response is still almost linear, despite the DC offset from the amplifying beam.

4. Instrument Function

Whereas the surface response function addresses the surface phenomenology, the Instrument Function addresses the properties of the optics and geometry of the instrument. The instrument function accounts for many physical properties of real optical systems, including the elliptical beam profile at the interface, optical aberrations, and aperture stops. Such a model of the experimental geometry is essential for accurately determining surface properties, particularly where the peaks are not so well separated.

To guarantee TIR, whose minimum angular condition depends on the fluids, the incident principal ray is inclined to

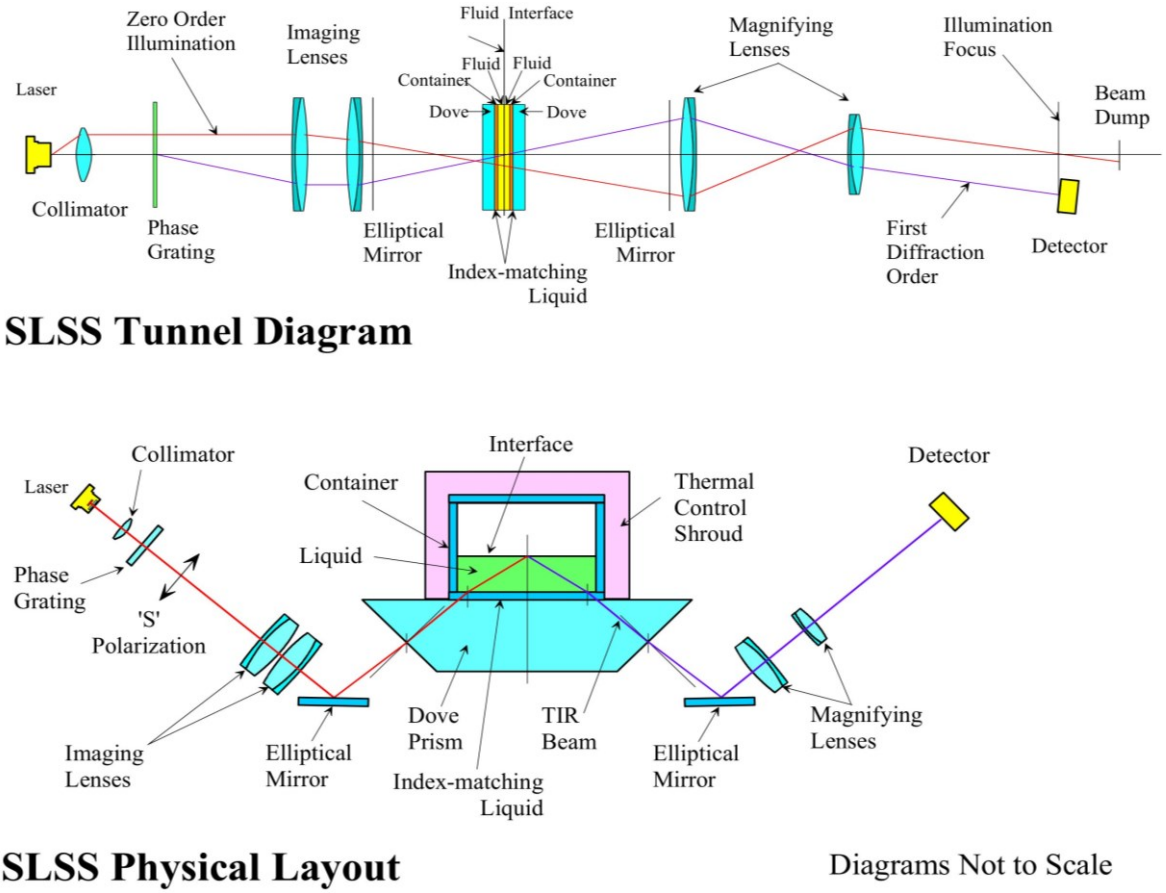

Figure 4. SLSS tunnel diagrams (upper) and schematic component layout (lower).

the surface by greater than 58 degrees, sufficient for most common fluids (**Figure S1** in Supplementary Materials). The TIR condition is insensitive to polarization. The orientation of the fringes with respect to the major axis of the elliptical footprint determines the extent to which an instrument function improves the results. This improvement depends strongly on the selectivity of $\vec{k}$, which increases with the number of illuminated fringes:

$$N = \frac{k\,D}{2\,\pi} \qquad (6)$$

where k is related to the fringe spacing $s = 2\,\pi/k$ and D is the Gaussian beam diameter at the $1/e^2$ intensity points normal to the fringes [45]. An instrument function always improves accuracy and is essential for $N < 50$, where too few fringes are imaged in the elliptical footprint at the surface [7,39,46].

More details about the instrument function are found in Section S4 of the Supplementary Materials.

5. Software

Data compression by correlation was universal in earlier systems, traditionally by hardware correlators, all of which suffered from some limitations.

Software performs necessary functions: First, archival storage of the full digitized data stream. This allows subsequent processing by different methods without the conventional real-time data compression and loss of information. Second, the signal, correlation function, and power spectrum can be viewed in effectively real-time to diagnose experimental problems such as contamination, improper alignment, and mechanical vibrations. The recorded data can also be segmented to watch the system evolve over time or to demonstrate its constancy.

Further details relevant to the design and implementation of functional software can be found in Section S5 of the Supplementary Materials.

6. Sample Data

The typical $\vec{q}$ explored by this SLSS is a small range around 500/cm or 1000/cm. For this range of $\vec{q}$, dispersion relations for 'low-viscosity' fluids predict power spectra enough displaced from 0 Hz, to mitigate any effects from unaddressed low-frequency contributions (Sections 2 and 5). For higher viscosity fluids the Instrument Function becomes relatively more important as surface tension and viscosity become increasingly difficult to separate. Here, we present

Sample	Y_1	y^*	$\gamma_{Lorentz}$	γ_{SRF}	γ_{SRF+IF}	γ_{Lit}	$\eta_{Lorentz}$	η_{SRF}	η_{SRF+IF}	η_{Lit}
Acetone	0.98	1949	22.79	23.211	23.302±0.032	23.32±0.10	0.31	0.35	0.33	0.34±0.18
Pentane	0.98	1506	15.70	16.043	16.018±0.025	16.02±0.15	0.26	0.28	0.24	0.23±0.16
Isopropanol	0.71	30	14.94	21.336	21.306±0.056	21.32±0.13	2.57	2.51	2.45	2.43±0.11

Table 1. Surface tension and viscosity from Lorentzian fits and SRF, without and with the Instrument Function (IF), for different materials (Y_1, y^*) with $N = 40$. Literature values from [25], and its references, with uncertainties based on their scatter.

typical data for fluids whose viscosity is low enough to be considered underdamped, i.e., $y^* \gg 0.58$.

6.1. Necessity of the Surface Response Function

Although commonly applied, the Lorentzian fit is not wholly adequate, because it does not account for all the hydrodynamic terms and worsens further as viscosity increases (Section 2.3). Here, we use isopropanol as an exemplary system to compare the Lorentzian approximation with the full SRF **without** the Instrument Function applied.

Figure 5 shows that the peak position and width are less well fit by the Lorentzian, which is fold-symmetric, than by the SRF, which is not. The SRF accounts for the skewness and other, higher-order, effects caused by the stream function [39], which are ignored in many historical approximations. The residuals in **Figure 5** show the significant improvement from applying a more comprehensive SRF, even though the Instrument Function may still be desirable.

Table 1 shows measurements at 19.95 °C with a 1000/cm grating, 1 µs sampling time, and 5-minute experiment duration. Using the same Instrument Function, this table indicates the significance of including the SRF compared with the oversimplified Lorentzian approximation whose fit results in an underestimate of surface tension that worsens as Y_1 decreases. The data in **Figure 5** appears negatively skewed, which causes the centre frequency of the Lorentzian fit to shift toward lower frequencies that correspond to lower surface tension values [47].

6.2. Applying the Instrument Function

The Instrument Function compensates for the effects of finite beam size and aperture, angle of incidence, and other optical properties (Section 4). Its application improves the SRF fit mostly in the width and shape of the spectrum.

The Instrument Function further improves the SRF fit rms residuals by a factor of ~10, as shown in **Figure 6**. With the 500/cm grating and a beam diameter of 0.256 cm, yielding $N = 20$, disabling the Instrument Function causes a 0.45% error in the surface tension and 45% error in viscosity. For the 1000/cm grating with $N = 40$, disabling the Instrument Function causes a 0.18% error in surface tension and 12% error in viscosity. Increasing N reduces the need for an instrument function, although its application is always

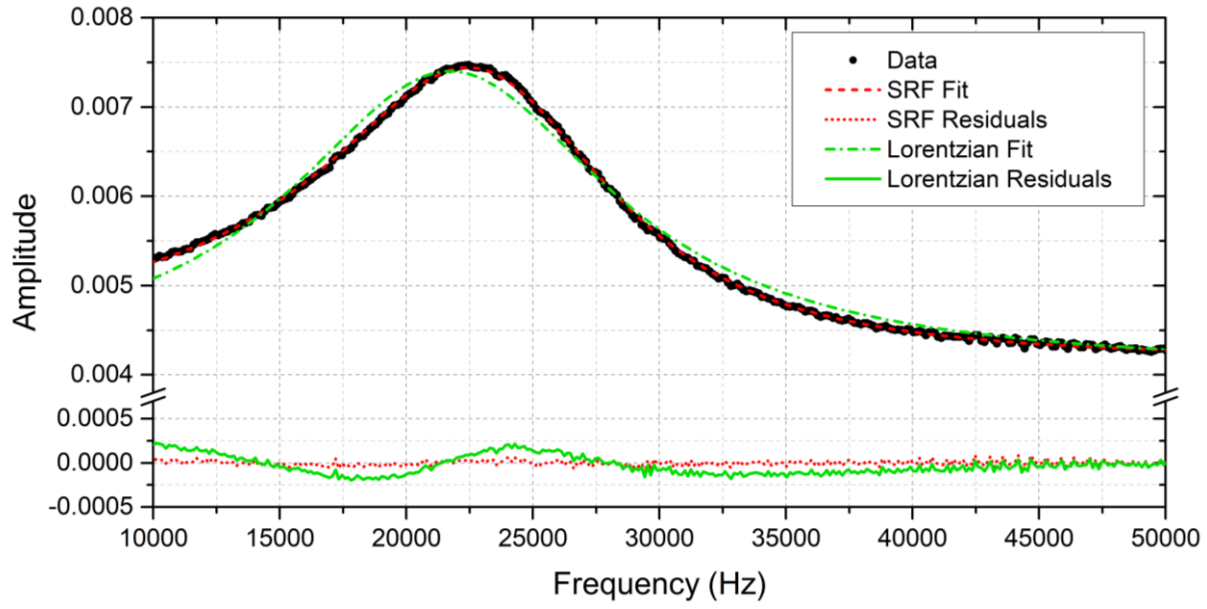

Figure 5. Comparison of power spectral data fitted for pure isopropanol with the Surface Response Function (SRF) and Lorentzian. $N = 40$, no instrument function. Data at 19.95 °C with a 1000/cm grating, 1 µs sampling time, and 5-minute experiment.

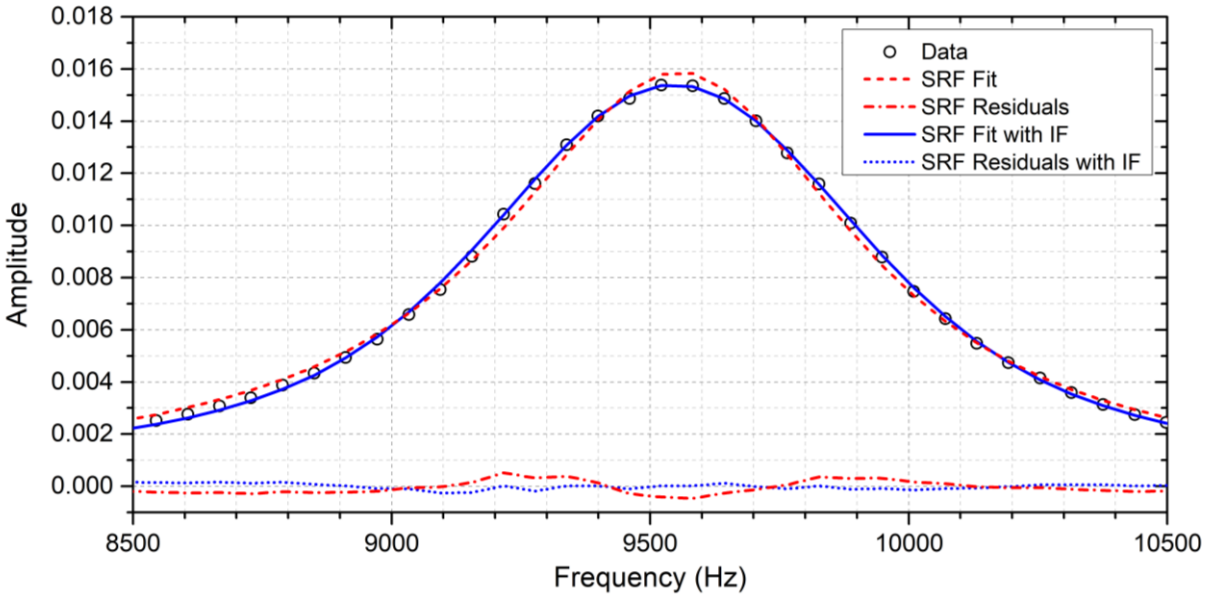

Figure 6. Comparison of power spectral data for pure acetone fitted with the Surface Response Function (SRF), $N = 20$, with and without the Instrument Function (IF). Data at 19.95 °C with a grating of 500/cm, 1 µs sampling time, and 5-minute experiment.

beneficial. As viscosity increases, applying an instrument function becomes more necessary.

6.3. Resistance to Sloshing

Mechanical vibrations induce sloshing, which is an oscillatory distortion of the fluid-fluid interface on a spatial scale larger than a small fraction of the illuminated footprint. Its angular effects are to change the portion of the scattered light amplified and sampled by the detector. In the case implemented in this apparatus, $\vec{k}$ is the selection mechanism for that part of the $\vec{q}$ angular spectrum to be examined. In this case of TIR, light is reflected by twice the angle of the slope of the surface topography. Even if sloshing changes the mean surface inclination, the angular difference between the values of $\vec{k}$ and $\vec{q}$ remains the same, avoiding error as long as the amplifying beam remains fully on the detector. This advantage holds under two assumptions. First, the optics must be of sufficiently high quality so that the area of the amplifying beam is small compared with the detector and, even more restrictively, that the maximum displacement due to sloshing should not move it off the detector. Second, the light scattered onto the detector from the main illumination beam must be insignificant compared to the coherently amplified light. This typically constrains the accuracy of the observed $\vec{q}$, whose signal intensity arises from the integral of the sum of incident fields averaged over the detector and is not linear because of the strong $\vec{q}$ dependence on angle. This is worse when the grating spot is less tightly focused.

Although efforts to reduce vibration are desirable, mitigating its effects by design has proven more successful. The primary detrimental effect of sloshing is caused by angular redirection of the reflected beams, more specifically, the variation of the centre of the amplifying beam with respect to the detector, which (even) antivibration tables cannot totally eliminate. Although sloshing moves both the amplifying and scattered beams together, avoiding frequency error by keeping $\vec{q} - \vec{k}$ constant, too great an angular deflection can move the illumination partially or completely off the detector, introducing potentially large amplitude modulation and/or transient signal loss. Reducing the diameter of the amplifying beam to near diffraction-limited while retaining order separation, ameliorates this effect, as would a larger detector, but this also increases noise and introduces a possibly significant broadening and skewing of the selectivity of $\vec{k}$.

Figure 7 shows how well-optimised optics improves the signal peak in the power spectrum of acetone. Data were recorded at 19.95 °C with a grating of 500/cm, a sampling time of 1 µs for an experiment duration of 10 minutes, and with 24 dB/octave roll-off 300 Hz high-pass and 250 kHz low-pass anti-aliasing filter. Moderate sloshing was imposed by the pump, Julabo F12, which circulated water to maintain temperature inside the thermal shroud, and is therefore considered a normal operating condition. More serious sloshing was induced by mechanical vibration from an unbalanced fan bolted to the floating optical bench. This resulted in vibrations with four times the acceleration, but similar frequency spectra, compared to that observed on a countertop in ambient conditions (Supplementary Materials S6). The lower black (solid) and red (dotted) curves show the effects of moderate and severe sloshing respectively with optics that proved less than satisfactory. With the improved

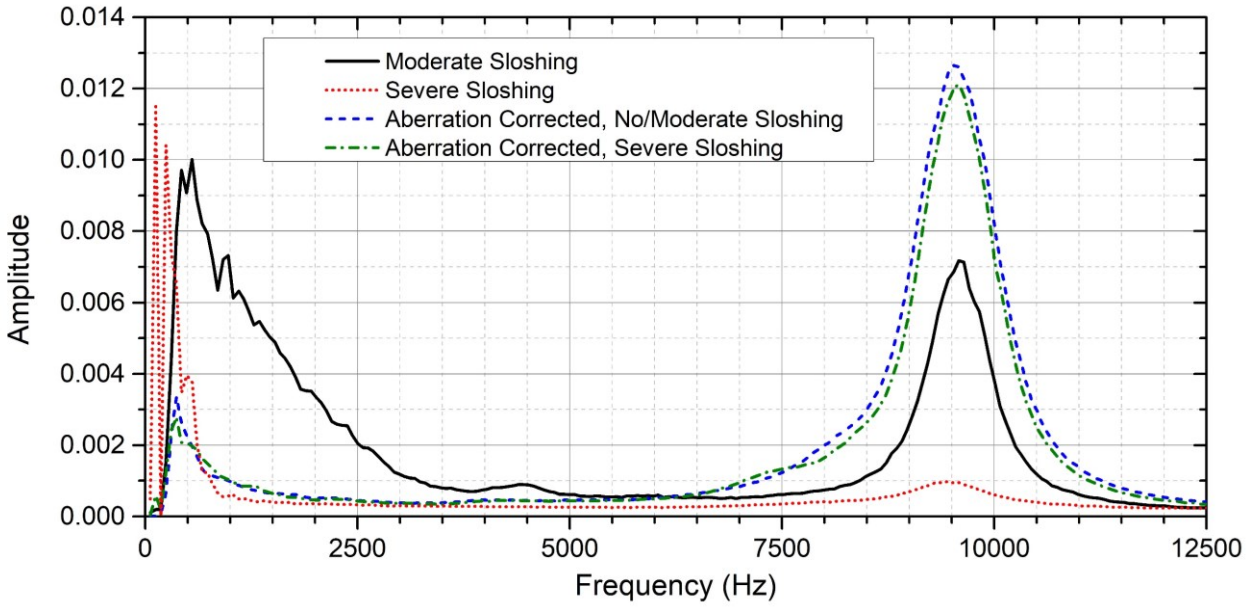

Figure 7. Comparison of the effect of sloshing behaviour on the power spectrum with and without optimized optics. Data at 19.95 °C with $N = 20$, 1 μs sampling time, and 10-minute experiment.

optics, the blue (upper dashed) line represents indistinguishable results for both ambient and moderate imposed vibration – essential immunity to vibration-induced sloshing. The slightly lower green (intermittent, dash-dotted) shows only marginally worse behaviour under extreme vibration. Our data indicate that excellent results may be obtained in the presence of vibration-induced sloshing. Overcoming the detrimental effects of vibration, a former major drawback of this technique, makes the experiment both practical and robust [1].

6.4. Typical Data

Low viscosity fluids such as pentane, acetone, and water, show sufficiently underdamped ripplons at either 500/cm or 1000/cm values of $\vec{q}$ to have spectral peaks clearly separated from zero (**Figure 2**).

Pentane and 2-methylpentane differ in surface tension by ~1.25 mN/m. **Figure 8** shows three distinct mixtures with volume fractions of pure pentane, pure 2-methylpentane, and a mixture of 40% pentane to 60% 2-methylpentane by volume. The liquids were compared with analytic standards for purity and were verified to within experimental uncertainty (see Supplementary Materials S6). Thirty analogous measurements by SLSS over the complete range of volume fraction are sufficiently precise to distinguish surface tensions from mixtures of the two fluids to greater than 0.05 mN/m. The disparity between accuracy and precision is largely based upon uncertainty of initial or changing position of the surface itself. For example, if evaporation moves the surface position below the optimal focus of the grating, the contrast and distance between fringes both decrease, changing the calculated values of thermophysical parameters. The variance of the surface tension measurements is 0.002 mN/m, which suggests a limiting uncertainty for this SLSS instrument.

Conclusions

In summary of the results section, we confirm four observations: (i) a more inclusive surface response function more accurately models fluid surfaces than a Lorentzian fit, (ii) an instrument function always improves accuracy, which may be further improved for higher viscosities with the inclusion of more complete properties of the apparatus, (iii) likely accuracy may be predicted from the known boundary conditions imposed by the apparatus, and the extent to which the details of the fitting model include all of the phenomenological variables, and (iv) this improvement of measurement precision and accuracy allows a more comprehensive analysis of the behaviour of fluid interfaces, introducing the possibility of measuring formerly inaccessible effects. Our measured values are well within the scatter of the literature values in **Table 1**.

The instrument described here combines many independent improvements to overcome common limitations of dynamic surface light scattering spectroscopy. Design enhancements make the instrument largely immune to sloshing. The interface measurement is made in a mechanically, chemically, and thermally controlled environment without physical contact.

Robust design assures that the initial alignment is simple and retained. The acquired signal is stored for further analysis. The Surface Response and Instrument functions are combined into a comprehensive model that allows recovery of

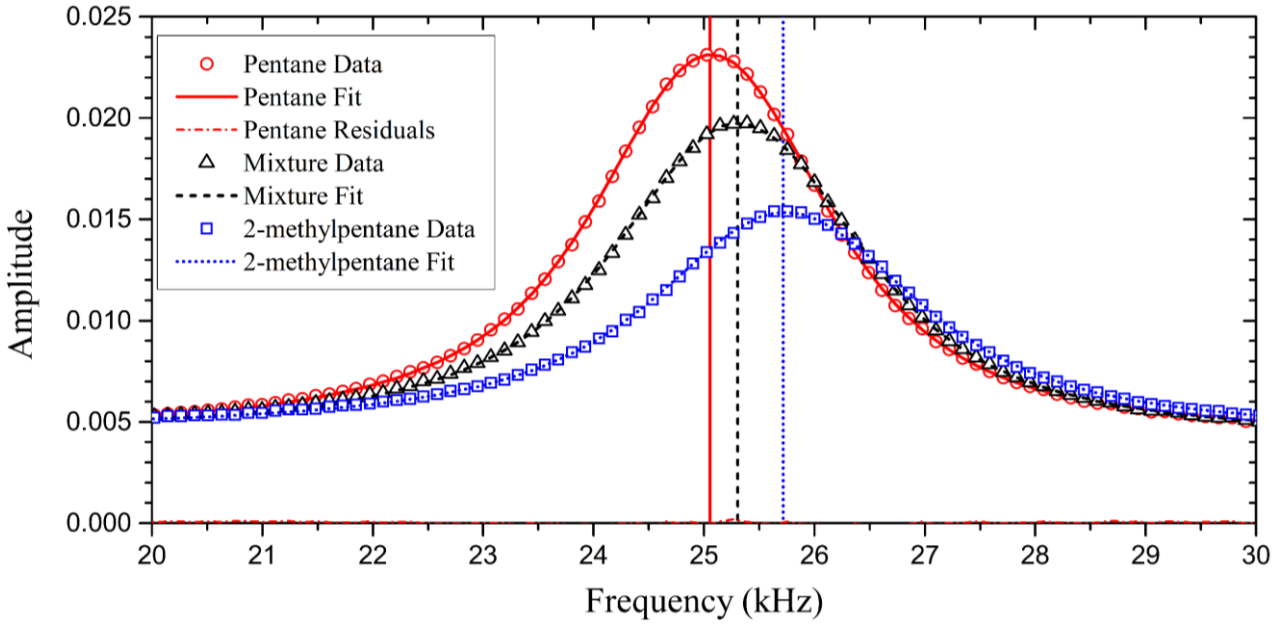

Figure 8. Three samples are shown at 19.95 °C with a 1000/cm grating, 1 μs sampling time, and 10-minute experiment duration. 'Mixture' is of 40% pentane to 60% 2-methylpentane by volume. The Surface Response Function (SRF), corrected by the Instrument Function, provides fits with sufficient resolution to distinguish surface tensions separated by less than 0.05 mN/m.

phenomenological properties. While the design has some subtleties (see Supplementary Materials), simplicity of implementation and use yields accurate measurements that accord with published sources. This spectrometer is now practical for use in many laboratories.

We show experimental spectra for four fluids: pentane, 2-methylpentane, acetone, and isopropanol, whose viscosity is small enough to support underdamped ripplons. The power spectrum of fluctuations is shown to depend dominantly on the bulk viscosity and surface tension, with negligible effects from other surface visco-elastic effects.

The reported results are restricted to underdamped systems, where the detected peak in the measured spectrum is separated from zero frequency by much more than the combined widths of the zero and first-order spectra. We are currently working to broaden the range of applicability by replacing some of the assumptions with a deeper understanding of the physics upon which they are based (see Supplementary Materials).

Acknowledgements

Scattering Solutions, Inc provided the instrument design, software, and some equipment used in the experiment.

This work was partially supported by the National Science Foundation under Grant No. DMR-1709985. This work was completed while EKM served at the National Science Foundation.

Data Availability Statement

All data that support the findings of this study are included within the article (and any supplementary files).

ORCID iDs

1 Angelo Visco http://orcid.org/0000-0002-9369-4093
2 Alan Baldwin http://orcid.org/0000-0003-3005-714X
3 Alexander Belgovskiy http://orcid.org/0000-0003-0186-7522
4 J. Adin Mann http://orcid.org/0000-0002-8687-5611
5 William Meyer http://orcid.org/0000-0002-2474-7630
6 Anthony Smart http://orcid.org/0000-0003-2721-5995
7 Nabin Thapa http://orcid.org/0000-0002-9801-400X
8 Elizabeth Mann http://orcid.org/0000-0002-0020-5132

References

[1] Langevin D 2021 Light scattering by liquid surfaces, new developments *Adv. Colloid Interface Sci.* **289** 11

[2] Adamson A W and Gast A P 1967 Capillarity *Physical Chemistry of Surfaces* (New York: John Wiley & Sons, Inc.) pp 10–40

[3] Berry J D, Neeson M J, Dagastine R R, Chan D Y C and Tabor R F 2015 Measurement of surface and interfacial tension using pendant drop tensiometry *J. Colloid Interface Sci.* **454** 226–37

[4] Saad S M I and Neumann A W 2016 Axisymmetric Drop Shape Analysis (ADSA): An Outline *Adv. Colloid Interface Sci.* **238** 62–87

[5] Bouchiat M A and Meunier J 1969 Light Scattering from Surface Waves on Carbon Dioxide Near the Critical Point *Phys. Rev. Lett.* **23** 752–5

[6] Meyer W V, Mann J A and Wegdam G H 2006 Surface response functions for a thin-film between fluids with infinite boundaries and for a fluid-fluid interface between finite boundaries *Appl. Opt.* **45** 2174–85

[7] Meyer W V, Wegdam G H, Fenistein D and Mann J A 2001 Advances in surface-light-scattering instrumentation and analysis: noninvasive measuring of surface tension, viscosity, and other interfacial parameters *Appl. Opt.* **40** 4113

[8] Adamson A W and Gast A P 1967 The Nature and Thermodynamics of Liquid Interfaces *Physical Chemistry of Surfaces* (New York: John Wiley & Sons, Inc.) pp 74–7

[9] Hansen R S 1962 Thermodynamics of interfaces between condensed phases *J. Phys. Chem.* **66** 410–5

[10] Turkevich L A and Mann J A 1990 Pressure Dependence of The Interfacial Tension between Fluid Phases. 1. Formalism and Application to Simple Fluids *Langmuir* **6** 445–56

[11] Rowlinson J S and Widom B 1989 Density fluctuations and their correlation *Molecular Theory of Capilarity* (New York: Oxford University Press) pp 115–22

[12] Aarts D G A L, Schmidt M and Lekkerkerker H N W 2004 Direct Visual Observation of Thermal Capillary Waves *Science* **304** 847–50

[13] Pouchelon A, Meunier J, Langevin D and Cazabat A M 1980 Light scattering from oil-water interfaces : measurements of low interfacial tensions *J. Phys. Lett.* **41** 239–42

[14] Hård S and Neuman R D 1987 Accurate laser light-scattering measurements of capillary waves *J. Colloid Interface Sci.* **115** 73–86

[15] Sauer B B, Chen Y L, Zografi G and Yu H 1988 Surface light scattering studies of dipalmitoylphosphatidylcholine monolayers at the air/water and heptane/water interfaces *Langmuir* **4** 111–7

[16] Dorshow R B, Hajiloo A and Swofford R L 1988 A surface laser-light scattering spectrometer with adjustable resolution *J. Appl. Phys.* **63** 1265–78

[17] Dorshow R B and Swofford R L 1989 Application of surface laser-light scattering spectroscopy to photoabsorbing systems: The measurement of interfacial tension and viscosity in crude oil *J. Appl. Phys.* **65** 3756–9

[18] Dorshow R B and Swofford R L 1990 An adjustable-resolution surface laser-light scattering spectrometer and its application to the measurement of interfacial tension and viscosity in crude oil systems *Colloids Surf.* **43** 133–49

[19] Sharpe D and Eastoe J 1995 Surface Light Scattering from Mixed Surfactant-Oil Monolayers *Langmuir* **11** 4636–8

[20] Earnshaw J C and Sharpe D J 1996 Surface viscoelasticity of a foam-forming solution *J. Chem. Soc. Faraday Trans.* **92** 611

[21] Eastoe J and Sharpe D 1998 Surface light scattering from cationic surfactant films *Colloids Surf. Physicochem. Eng. Asp.* **143** 261–71

[22] Atsumi Ozawa A O and Akiko Minamisawa A M 1997 Noncontact Measurement of Surface Tension by Ripplon Light Scattering Spectroscopy *Jpn. J. Appl. Phys.* **36** 2951

[23] Monroy F, Ortega F and Rubio R G 1999 Rheology of a Miscible Polymer Blend at the Air−Water Interface. Quasielastic Surface Light Scattering Study and Analysis in Terms of Static and Dynamic Scaling Laws *J. Phys. Chem. B* **103** 2061–71

[24] Alexander M and Richards R W 2000 Capillary Wave Phenomena at the Air Interface of Aqueous Dispersions of a Linear Polystyrene−Poly(ethylene oxide) Diblock Copolymer *J. Phys. Chem. B* **104** 9179–85

[25] Milling A J, Richards R W, Baines F L, Armes S P and Billingham N C 2001 Surface Viscoelastic Parameters of Poly((dimethylamino)ethyl methacrylate−methyl methacrylate) Diblock Copolymer Solutions: pH Dependence of the Evolution of the Equilibrium Values *Macromolecules* **34** 4173–9

[26] Kim C and Yu H 2003 Surface Rheology of Monolayers of Triblock Copolymers of PEO and PPO: Surface Light Scattering Studies at the Air/Water Interface *Langmuir* **19** 4460–4

[27] Cicuta P and Hopkinson I 2004 Recent developments of surface light scattering as a tool for optical-rheology of polymer monolayers *Colloids Surf. Physicochem. Eng. Asp.* **233** 97–107

[28] Tin P and de Groh III H C 2004 Surface Tension and Viscosity of Succinonitrile– Acetone Alloys Using Surface Light Scattering Spectrometer *Int. J. Thermophys.* **25** 1143–53

[29] Muñoz M G, Encinar M, Bonales L J, Ortega F, Monroy F and Rubio R G 2005 Surface Light-Scattering at the Air−Liquid Interface: From Newtonian to Viscoelastic Polymer Solutions *J. Phys. Chem. B* **109** 4694–9

[30] Rojas O J, Neuman R D and Claesson P M 2005 Viscoelastic Properties of Isomeric Alkylglucoside Surfactants Studied by Surface Light Scattering *J. Phys. Chem. B* **109** 22440–8

[31] Hilles H M, Sferrazza M, Monroy F, Ortega F and Rubio R G 2006 Equilibrium and dynamics of Langmuir monolayers when the interface is a selective solvent: Polystyrene-b-poly(t-butyl acrylate) block copolymers *J. Chem. Phys.* **125** 074706

[32] Oki K and Nagasaka Y 2009 Measurements of anisotropic surface properties of liquid films of azobenzene derivatives *Colloids Surf. Physicochem. Eng. Asp.* **333** 182–6

[33] Koller T M, Prucker T, Cui J, Klein T and Fröba A P 2019 Interfacial tensions and viscosities in multiphase systems by surface light scattering (SLS) *J. Colloid Interface Sci.* **538** 671–81
[34] Koller T M, Yan S, Steininger C, Klein T and Fröba A P 2019 Interfacial Tension and Liquid Viscosity of Binary Mixtures of n-Hexane, n-Decane, or 1-Hexanol with Carbon Dioxide by Molecular Dynamics Simulations and Surface Light Scattering *Int. J. Thermophys.* **40** 79
[35] Cui J, Bi S, Fröba A P and Wu J 2021 Viscosity and interfacial tension of n-heptane with dissolved carbon dioxide by surface light scattering (SLS) *J. Chem. Thermodyn.* **152** 106266
[36] Sakai K 2021 Introduction to rheometry for researchers of ultrasonics *Jpn. J. Appl. Phys.* **60** SD0801
[37] Kerscher M, Fröba A P and Koller T M 2021 Viscosity and Surface Tension of Benzene at Saturation Conditions from Surface Light Scattering *Int. J. Thermophys.* **42** 159
[38] Zhang X, Zhao G, Yin J and Ma S 2022 Experimental investigation of saturated liquid kinematic viscosity and surface tension of two isomeric refrigerants trans-1,1,1,4,4,4-hexafluoro-butene (R1336mzz(E)) and cis-1,1,1,4,4,4-hexafluoro-butene (R1336mzz(Z)) by surface light scattering *Fluid Phase Equilibria* **559** 113468
[39] Mann J A, Crouser P D and Meyer W V 2001 Surface fluctuation spectroscopy by surface-light-scattering spectroscopy *Appl. Opt.* **40** 4092
[40] Langevin D 1992 *Light scattering by liquid surfaces and complementary techniques* vol 41 (New York: Marcel Dekker, Inc.)
[41] Wagner F 1973 Scattering of light by thermal ripplons on superfluid helium *J. Low Temp. Phys.* **13** 317–30
[42] Lading L, Mann J A and Edwards R V. 1989 Analysis of a surface-scattering spectrometer *J Opt Soc Am A* **6** 1692–701
[43] Hanson S G, Lindvold L R and Lading L 1996 A surface velocimeter based on a holographic optical element and semiconductor components *Meas. Sci. Technol.* **7** 69–78
[44] Smith J W 2000 *Modern Optical Engineering: The Design of Optical Systems* (New York: McGraw-Hill)
[45] Kogelnik H and Li T 1966 Laser Beams and Resonators *Appl. Opt.* **5** 1550–67
[46] Meyer W V 2002 *Volume and Interface Studies of Complex Liquid Media* (University of Amsterdam)
[47] Yaws C L 2009 Transport Properties of Chemicals and Hydrocarbons *Transport Properties of Chemicals and Hydrocarbons* (Norwich, NY: William Andrew Inc.)